Journal of The Electrochemical Society, **164** (13) F1301-F1306 (2017)
0013-4651/2017/164(13)/F1301/6/$37.00 © The Electrochemical Society

Enhanced Thermal Stability of a Gadolinia-Doped Ceria Capped Metal Electrode for Durable Low-Temperature Solid Oxide Fuel Cells

Soonwook Hong,[a] Seongkook Oh,[b] Hyong June Kim,[b] Yonghyun Lim,[a] Jihwan An,[b] and Young-Beom Kim[a,c,z]

[a]*Department of Mechanical Convergence Engineering, Hanyang University, Seongdong-gu, Seoul, 133-791, Korea*
[b]*Department of Manufacturing Systems and Design Engineering (MSDE), Seoul National University of Science and Technology, Korea*
[c]*Institute of Nano Science and Technology, Hanyang University, Wangsimni-ro, Seoul 133-791, Korea*

A gadolinia-doped ceria (GDC) capping layer was fabricated on a metal Pt cathode via a sputtering technique to enhance the thermal stability and oxygen-reduction reaction (ORR) kinetics. By varying the thickness of the GDC thin film on the Pt cathode, we fabricated thermally durable low-temperature solid oxide fuel cells (LT-SOFCs) on porous anodized aluminum oxide (AAO) substrates while securing very high performance. The GDC protective layers subsequently mitigated the agglomeration of the Pt morphology by hindering the coarsening of metal grains, and enhanced the cathodic kinetics as a result of the increased TPB density at the Pt-electrolyte interface. Enhanced performance of fuel cells and thermo-stable behavior with the GDC capping layer were demonstrated by employing transmission electron microscopy (TEM) and electrochemical analysis. An enhanced peak power density of 258 mW/cm^2 was obtained with a degradation of 56.4% of the Pt cathode over 25 hours of operation at 450°C.

Manuscript submitted July 20, 2017; revised manuscript received September 15, 2017. Published September 26, 2017.

Efforts to develop solid oxide fuel cells (SOFCs) have progressed over the past few decades for their high energy conversion rate, diversity of fuels, and no pollutant emissions. However, SOFCs typically require high operating temperatures (800–1000°C) because the ceramic electrolyte barely has a sufficient ionic conductivity in this temperature region. Moreover, this high operating temperature leads to thermally unstable behavior of SOFCs, deterioration of the sealing degree, and in particular, degradation of the electrode. Several approaches have been implemented to lower the operating temperature between 300°C and 500°C to alleviate the issues mentioned above while maintaining reasonably high performance.[1,2] One of them is thin film fabrication of an electrolyte in which a thickness less than one micrometer to mitigate the increased ohmic resistance at lower temperature regime.[3–10] At that temperature regime, a significant drop of the oxygen ion conductivity is obtained for the ceramic electrolyte. Thin film SOFCs (TF-SOFCs) are able to compensate for the lowered ionic conductivity by reducing the thickness of electrolyte with a decreased ohmic loss.

Other than ceramic electrolyte for ionic conduction, conventional cathode materials for high temperature SOFCs typically use a mixed ionic-electronic conductor such as $La_{1-x}Sr_xCo_{1-y}Fe_yO_3$, $La_{1-x}Sr_xCoO_3$, $Ba_{1-x}Sr_xCo_{1-y}Fe_yO_3$, or $La_{1-x}Sr_xMnO_3$.[11–17] In low temperature regions, however, these materials show a dramatic drop of catalytic activity due to their sensitivity to operating temperature. In this sense, a porous platinum (Pt) cathode has been employed for low temperature SOFCs (LT-SOFCs) as it is the best candidate material for the oxygen reduction reaction (ORR) for its exceptional catalytic activity at the low operating temperature regime.[8,18–22] The Pt electrode as a cathode layer is usually deposited via a thin film fabrication process such as physical vapor deposition (PVD) to achieve a porous morphology. The PVD method readily controls the morphology and structure of thin films, securing the porosity at the nanoscale as they can increase the triple-phase boundary (TPB) density, which is considered as the actual electrochemical reaction site for the ORR. However, one of the major issues in the use of Pt electrodes is morphological agglomeration, even in the low operating temperature (300–500°C) region.[23–27] Due to their highly porous nature of the thin film resulting in a high surface energy state, they readily agglomerate with each other and decrease the surface area during the operation of the fuel cell. This rapid morphological and structural degradation of the Pt electrode leads to a loss of the TPB density, which eventually results in a performance drop and thermal instability.

In earlier studies, the concept of an oxide-capping layer through a thin film fabrication process on the metallic electrode has been proposed, which plays a role in preventing the agglomeration of porous metal electrode for electrochemical stability and providing an enhanced catalytic reaction between the metal electrode and oxide-capping layer.[28–32] Most studies have introduced the fabrication of an oxide-capping layer with a noble thin film fabrication technique such as atomic layer deposition (ALD). Liu et al. suggested that depositing a zirconia capping layer on top of metal electrodes by ALD method plays a role as a thermal barrier and catalytic active layer.[30] Chang et al. also reported an yttria-stabilized zirconia (YSZ) coating on a porous Pt electrode by plasma-enhanced ALD for thermal stability and ORR activity enhancement.[32] The ALD technique is generally known for its highly conformal coating quality and precise thickness control as well as superb penetration of depth for porous thin films. At the early deposition stage of ALD, the synthesis starts from nucleation of the materials and following wetting behavior as the process cycle number increases. Utilizing the nucleated island-like morphology of thin film at the initial deposition step is highly useful to form a capping layer on metal electrodes. For increasing the TPB density of metal cathode as well as enhancing the thermal stability, however, the ALD technique has downside of relatively long process time and waste of materials which are related to the high fabrication cost. Despite the fact, ALD has been considered as the most suitable technique for fabrication of the nanoscale oxide-capping layers. PVD techniques including sputtering methods have also been demonstrated as excellent thin film techniques for the fabrication of TF-SOFCs. On the other hand, unlike the ALD or chemical vapor deposition techniques PVD processes have the line-of-sight growth characteristics resulting in a less conformal coating on the porous thin film structures and they usually form a columnar structured thin film.[33,34] Therefore, the sputtering technique has rarely been considered or utilized for the fabrication of an oxide-capping layer.[35,36]

It was recently revealed that the agglomeration of the thin-film porous Pt electrode mainly initiated from the top-part to the electrolyte interface.[37] This implies that the sputtering technique can also be a good candidate to fabricate an oxide-capping layer for stability enhancement. It is acceptable that sputtering technique able to hinder the agglomeration of metal electrode despite only deposition of top-part of Pt electrode due to the nature of PVD. Furthermore, it also suggests that the oxide-capping layer not only increases the thermal stability through sustainable morphology of the top electrode,

[z]E-mail: ybkim@hanyang.ac.kr

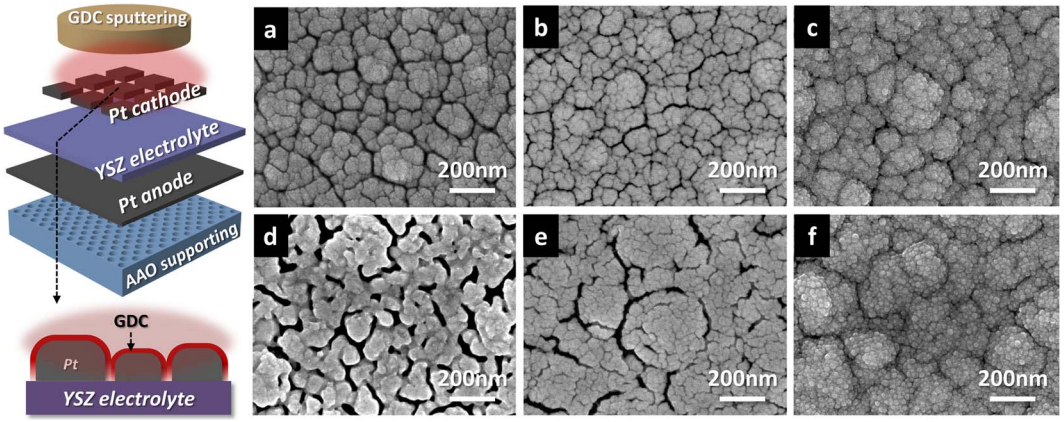

Figure 1. (left) Schematic of the fabrication of fuel cells and (right) top-view SEM images of the morphology before and after operation at 450°C of the (a, d) pristine Pt, (b, e) 15 nm thick GDC oxide-capped, and (c, f) 50 nm thick GDC oxide-capped cathodes.

but seemingly enhances the ORR kinetics by the penetrated GDC particles through the gap of nano-porous Pt from the initial step of the sputtering process.[35] It is regarded that this sputtering technique is able to overcome the issues related to the ALD technique such as wasting precursor materials and a relatively long deposition time.

In this work, we propose a method to produce an oxide-capping layer on a Pt cathode to enhance the thermal stability and ORR kinetics via a sputtering technique using gadolinia-doped ceria (GDC), which is normally considered as possessing higher ionic conductivity at lower temperature. TF-SOFC samples were fabricated on anodized aluminum oxide (AAO) nano-porous supporting structure. The performance of the fabricated oxide-capped fuel cells was significantly high in terms of the peak power density, 258 mW/cm^2 at 450°C. Furthermore, the fuel cells with an oxide-capping layer showed enhanced durability than the Pt cathode for more than 25 hours of continuous fuel cell operation at elevated temperature.

Experimental

To fabricate TF-SOFCs, 1 cm × 1 cm × 100 μm AAO (Synkera Technologies, Inc.) was used as a porous supporting structure with an average pore diameter of 55 nm. Onto this substrate, a porous Pt anode was deposited with a thickness of approximately 150 nm through sputtering at a DC power of 100 W and a working pressure of 10 Pa. Then, dense 500 nm thick YSZ was deposited on the Pt anode as an electrolyte using a sputtering process under an argon/oxygen flow rate of 20:3 sccm and a DC power of 90 W at a working pressure of 0.67 Pa. The Pt cathode was applied onto the YSZ electrolyte with a thickness of 100 nm and 1 mm × 1 mm active area under the same sputtering conditions employed in the anode fabrication. Finally, the GDC ($Gd_{0.1}Ce_{0.9}O_{2-x}$, RND Korea) oxide-capping layers were deposited on the porous Pt cathode with thicknesses of 15 nm and 50 nm on a Pt cathode employing sputtering conditions including an RF power of 60 W and an argon flow rate of 40 sccm under a working pressure of 0.67 Pa, as depicted in Figure 1.

The surface morphology of the fabricated GDC capped fuel cells was inspected using a scanning electron microscope (SEM, FEI Xl30, Sirion). Auger spectroscopy (PHI700Xi, AES700) was performed for elemental mapping of the surface composition of the GDC oxide-capping layer. Further morphological information and elemental mapping was characterized by using a transmission electron microscope (TEM, JRM-ARM200F, JEOL) by observing the cross-sectional morphologies of the GDC oxide-capping layer on the Pt cathode. For the preparation of TEM specimens, the fabricated GDC layer on Pt/YSZ/Pt fuel cells was mechanically ground and polished until it has the thickness of 15 μm. Then, ion milling was performed for electron transparency using a Gatan ion polishing system (PIPS691, Gatan Inc.). Argon ion beams biased with 5 keV were used to fabricate a hole in the center of the specimens with an incident angle of 6°. As a final process, reduced argon ion beams accelerated at 500 eV were applied to clean the sample surface.

The performance of the fabricated fuel cells was characterized by employing a custom-made micro-probe station which is able to sustain a constant temperature during the operation using a substrate heater. To set the fuel cell operation circumstance, we supplied hydrogen as a fuel with 20 sccm of flow rate to anode and exposed cathode to air for fueling oxygen at 450°C operation temperature. A Gamry potentiostat (Gamry Instrument Inc., FAS2) was used to deduce the polarization curves for each GDC oxide-capping layer sample. Electrochemical impedance spectroscopy (EIS) was employed to analyze the electrochemical performance across the frequency ranges from 1 MHz to 1 Hz at the operating temperature and the acquired data was analyzed using the Z-view software (Scribner Association Inc.). The stability analysis utilized a chronoamperometry method to measure the amperage with a biased voltage of 0.5 V during the entire operation time of about 25 hours.

Results and Discussion

Figure 1 shows top-view SEM images of the Pt cathode with or without the GDC oxide-capping layer before and after the fuel cell operation. The SEM images of the pristine Pt cathode fuel cell in Figures 1a, 1d suffered a harsh morphology degradation after the fuel cell operation for 25 hours and significant loss of TPB density. For quantitative analysis of porosity change, we performed image processing method which calculate the portion of trench for Pt cathode by contrasting white and black. The 15 nm thick GDC oxide-capped fuel cell also showed an aggregated morphology when comparing the images obtained before and after fuel cell operation (Figures 1b and 1e) by indicating its decreased porosity from 17.7 to 9.0. The GDC oxide-capped fuel cell with a 50 nm thickness demonstrated no noticeable morphological change during the fuel cell operation by indicating its lessened porosity from 4.75 to 2.52, as shown in Figures 1c and 1f. This oxide-capping layer is believed to impede the ripening process of the porous Pt cathode by covering up each grain of Pt at the top site of the cathode. Considering that Pt agglomeration is normally initiated with the top-end of the morphology, we speculated that the YSZ/Pt interface morphology suffered less aggregation, as confirmed by the SEM inspection of the 50 nm thick GDC capping electrode.

For comprehensive observation of the surface compositional distribution and qualitative capping degree for the GDC oxide-capping layer, auger spectroscopy measurements were performed using a top-view elemental mapping method. Figure 2a depicts the compositional mapping image for the pure Pt cathode, demonstrating that the most of the element is Pt. It was confirmed that the GDC oxide-capping layer was deposited with a greater thickness resulting in reduced Pt

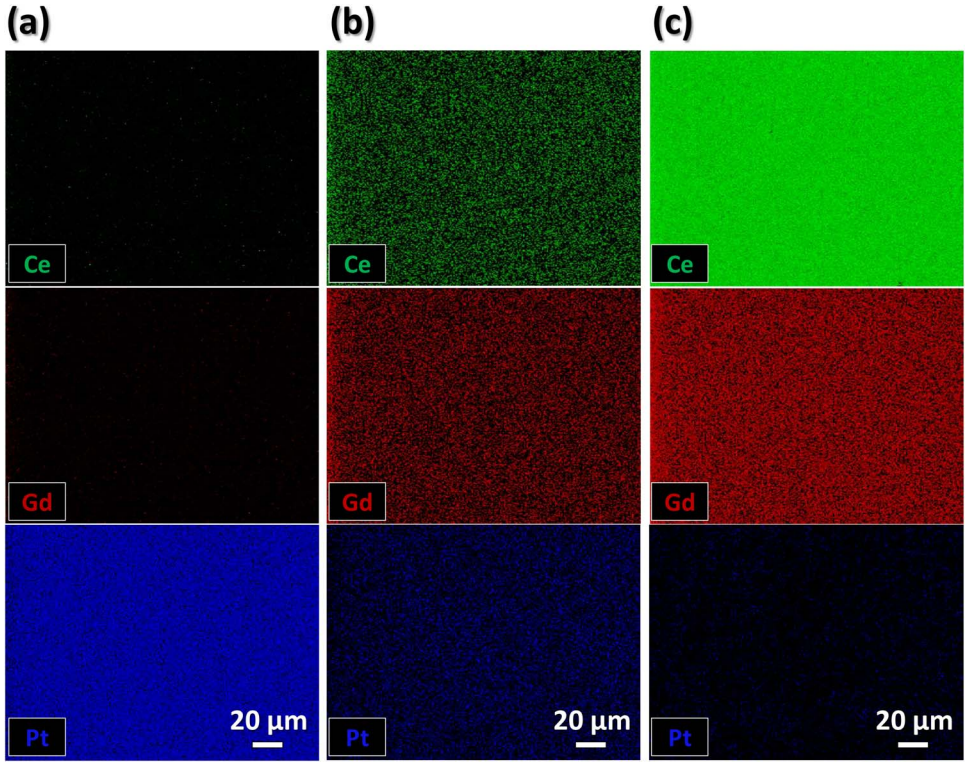

Figure 2. Auger elemental mappings of the fabricated fuel cells containing (a) pristine Pt, (b) 15 nm thick GDC oxide-capped, and (c) 50 nm thick GDC oxide-capped cathodes.

detection. Moreover, the element detection of gadolinium (Gd) and cerium (Ce) with different thicknesses of the GDC oxide-capping layer is also noticeable, where greater amounts of both Gd and Ce were observed with the 50 nm thick GDC layer compared to the thinner GDC layer. X-ray photoelectron spectroscopy (XPS) was also conducted to analyze the composition of GDC. The molar percentage of GDC capping layer with 15 and 50 nm-thick were indicated value of 10.59 and 10.98 respectively, which is almost same as the earlier result showing the highest ionic conductivity with 10 mol-percent.[35] Through the elemental mapping results obtained by auger spectroscopy, the GDC oxide-capping layers were clearly formed on the porous Pt cathode as a protective layer for thermal degradation providing enhanced thermal stability.

In order to further investigate the morphologies of the GDC oxide-capping layer, TEM was employed for the pristine Pt cathode and GDC oxide-capped electrode fuel cells. Figure 3a shows the cross-sectional morphology of the Pt cathode without a capping layer, and the morphologies with different thicknesses of protective GDC layers are shown in Figures 3b and 3c. Through this inspection, the actual thickness of the GDC oxide-capping layer and detailed morphology between the Pt and GDC layer were clearly observed. The GDC oxide-capping layers were successfully deposited on the uneven surface of the porous Pt cathode. However, the 15 nm thick GDC layer appears to not fully cover Pt, as observed in the interface morphology of the Pt/GDC layer. It seems to be no exposed portion of the Pt cathode, but it is assumed that the GDC capping layer with a 15 nm thickness is not enough to prevent the morphology change of the Pt cathode due to the lack of film thickness. Some researchers believe that the 15 nm film thickness is sufficient to sustain the morphological agglomeration of grains for the Pt cathode.[33] However, it is questionable to ensure the protective layer considering the ultra-thin thickness of the capping layer (15 nm). On the contrary, the TEM image of the 50 nm thick GDC oxide-capping layer appeared to fully cover the Pt cathode, ensuring the impediment of coarsening Pt grains. For detailed observation of enhanced ORR kinetics for the GDC oxide-capping layer, we analyzed the 50 nm thick GDC layer by elemental mapping using an energy dispersive X-ray (EDX) method, as presented in Figure 3d. The cross-sectional elemental mapping results revealed that the elements of Gd and Ce comprising the GDC capping layer are detected inside the Pt cathode structure, suggesting that sputtered GDC can partially penetrate into the columnar grains of the Pt cathode. The results also imply that a 50 nm thick GDC capping layer enhances the fuel cell performance and the cathode kinetics in terms of catalyzing ORR sites by increasing TPBs, as well as improving the thermal stability of the Pt cathode.

The current-voltage behaviors of the fabricated fuel cells on the AAO supporting structure presented in Figure 4a show that the pristine Pt cathode fuel cell had a peak power density of 142 mW/cm^2, while the GDC oxide-capped fuel cells with 50 and 15 nm-thick capping layers demonstrated peak power density values of 208 and 258 mW/cm^2 at 450°C, respectively. It is certain that these enhanced performances of the fuel cells resulted in the increased ORR sites from securing TPBs, as confirmed in the TEM-EDX analysis.[8,19,20] It is also appreciable that the performance of the fuel cell with the 15 nm thick GDC capping layer is higher than the sample with the 50 nm thick GDC capping layer. We speculate that the TPB density of the Pt-electrolyte interface is rather decreased with a thick GDC layer (i.e., 50 nm) due to the increased thickness, which blocks the activation of TPB sites by passivating the Pt cathode. However, with operating durations longer than 25 hours, the performance in terms of the peak power density for all of the fuel cell samples decreased due to degradation of the Pt cathode morphology under the operating conditions (Figure 4b). The fuel cell with the pure Pt cathode showed a peak power density of 13 mW/cm^2, signifying harsh agglomeration of the porous Pt cathode. It is reasonable for the performance degradation with pure Pt cathode fuel cell compared with earlier study.[30] Decreased performance caused by cathode degradation was also predicted upon inspection of the SEM images in Figure 1. The performance of the GDC capped fuel cells, on the other hand, demonstrated improved peak power densities of 20 and 77 mW/cm^2 with 15 and 50 nm thick GDC oxide capping

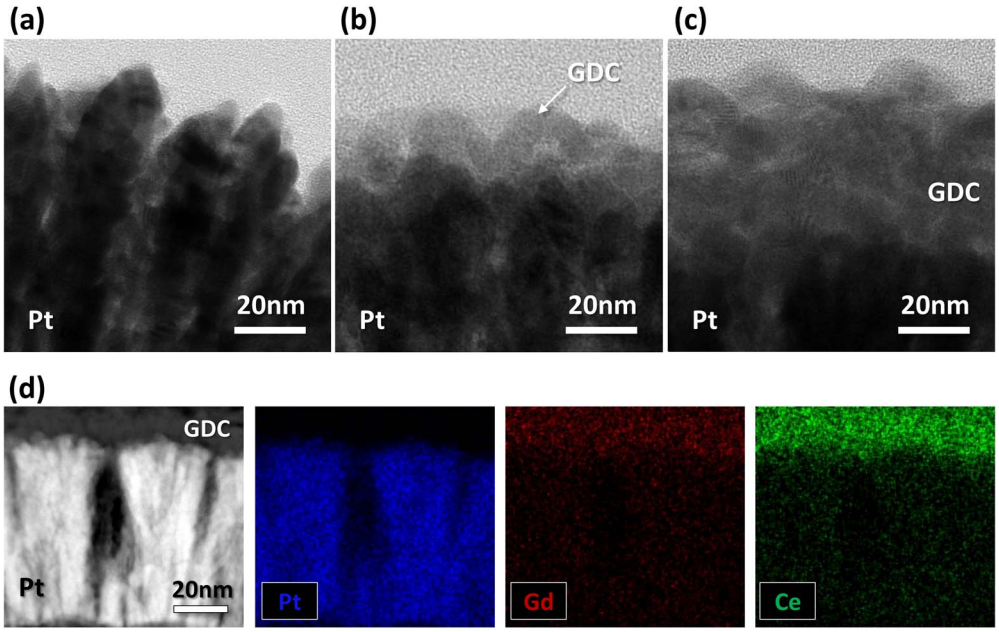

Figure 3. Bright-field cross-sectional TEM images of (a) pristine Pt, (b) 15 nm thick GDC oxide-capped, and (c) 50 nm thick GDC oxide-capped cathodes. (d) EDX elemental mapping results of the 50 nm thick GDC oxide-capping layer for certain elements.

layers, respectively, even after more than 25 hours of operation. It is noticeable that the decreased performance for the 15 nm thick GDC capping layer is more severe than that of the 50 nm thick capping layer, which is expected from the TEM analysis due to the lack of the capping degree on the Pt cathode. These performance results confirm that the 50 nm thick GDC oxide capping layer for the top section of the Pt cathode has considerable thermal stability by hindering degradation of the metal phase cathode, resulting in a superb performance even with the long term operation at elevated temperature condition.

For further investigation of the performance enhancement and degradation behavior, EIS analysis was performed for all of the fabricated fuel cell samples. Figure 5c shows representative Nyquist plots according to the different applied cell voltage conditions. As can be seen in the figure, the high-frequency loop is independent of the applied cell voltage conditions and this indicates that the loop corresponds to the ohmic resistance from ionic transport through the electrolyte. On the other hand, the low-frequency loop changes under different cell voltage conditions indicating that the loop corresponds to the electrode interface resistance.[9,19,20] It is seen that there are no distinct differences among the fuel cells, as depicted in Figure 5a. The identical first loops of the impedance spectra demonstrate no difference with regard to the GDC oxide-capping layer thickness due to orders of magnitude low thickness compared to the YSZ substrates used in each fuel cell sample. On the other hand, the low frequency loop, which is associated with electrode-electrolyte interface resistance, has different radii that vary with the various over-potential conditions. The second EIS loop of the pure Pt cathode fuel cell has the largest radius corresponding to Pt material without enhanced ORR kinetics, while the loops of the GDC capped fuel cells have radii that are about half that of the EIS loop of the pristine Pt sample. It is noted that the decreased radii of the arcs that are present correspond to the enhanced ORR kinetics; this is a result of the increased TPB density, as verified by the TEM-EDX analysis shown in Figure 3d. In particular, the 15 nm thick GDC capped fuel cell sample showed huge reduction of the radius of the second loop, which represents the most enhanced ORR kinetics with increased TPB sites. Nonetheless, after 25 hours of operation, it was observed that all of the fuel cells suffered from thermal degradation of the Pt cathode, as illustrated

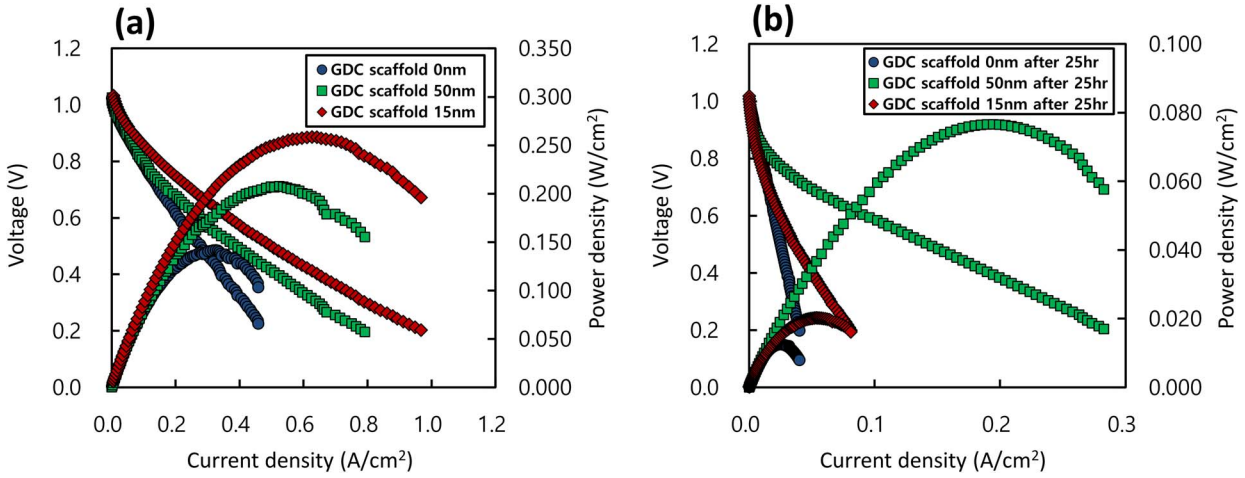

Figure 4. Polarization curves for each fuel cell fabricated on AAO substrates measured (a) at 450°C and (b) after 25 hours of operation.

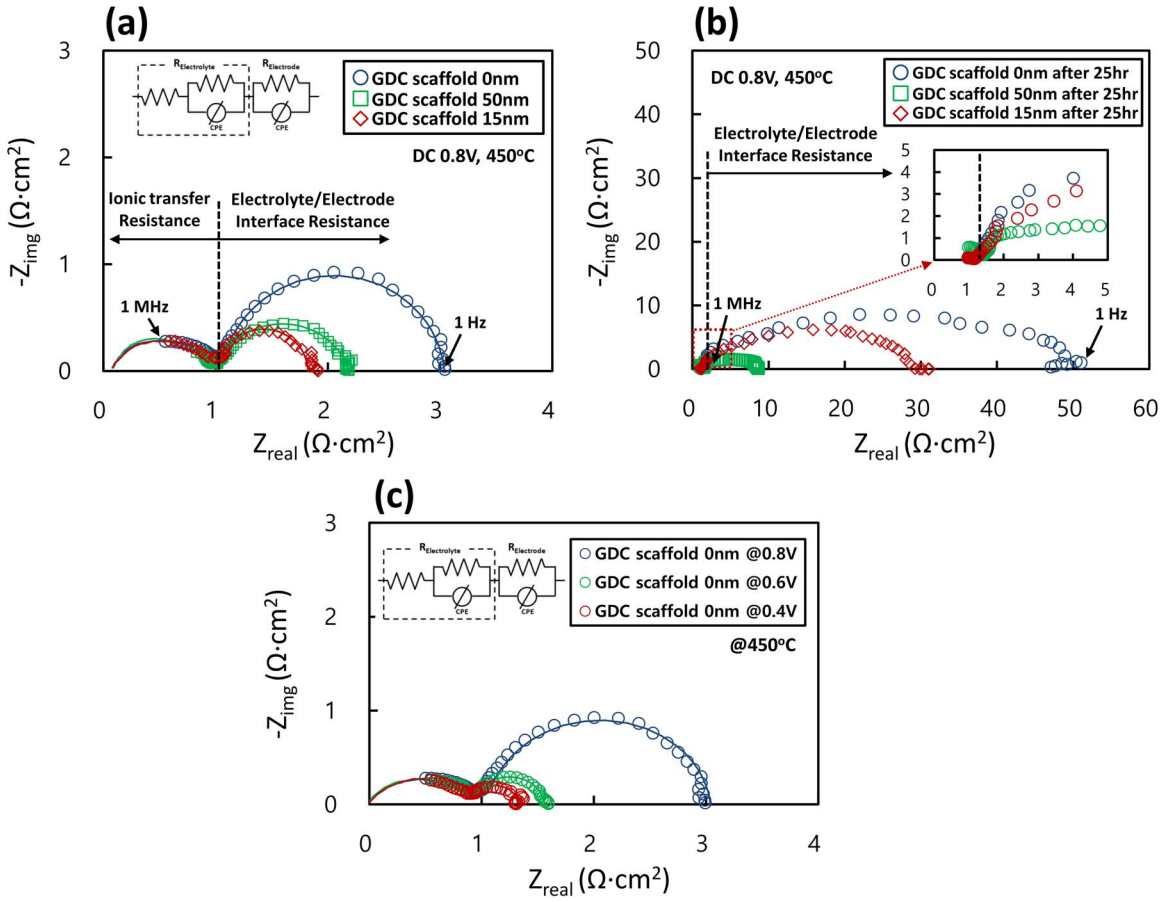

Figure 5. Impedance spectra of each fuel cell fabricated on AAO substrates measured (a) at 450°C and (b) after 25 hours of operation. (c) The impedance spectra with a varied DC bias voltage for fuel cell of pristine Pt cathode.

by the increased radius of the second EIS loop. The loop signaling the electrode-electrolyte interface resistance for the pristine Pt cathode immensely increased compared to the measured conditions. This increased interface resistance is ascribed to be due to the agglomeration of the Pt cathode, resulting in a loss of TPB sites due to the morphological thermal instability. In the case of the fuel cells with the GDC-capped cathode, however, it is seen that the increment of radius in terms of electrode interface resistance is less than that of the pure Pt case. In particular, the loop of the 50 nm thick GDC capping layer was merely enlarged its radius even after 25 hours of operation, implying enhanced thermal durability of the Pt cathode. This result means that the Pt cathode coated with 50 nm thick GDC thin film although suffered slight degradation at initial stage of operation due to process of lower the surface energy of Pt cathode using migration of its morphological evolution, but this morphological change is readily hindered by GDC capping layer resulting in less lost of TPB density. This phenomenon was well coincidence with previous studies for oxide capping layer using ALD technique.[30,31] Repeatedly, this enhanced thermo-stability for the Pt cathode is confirmed by the 50 nm thick GDC capping layer, resulting in a thermo-electrochemical sustainable protective layer.

For further investigation of the enhanced cathode-electrolyte surface kinetics, the exchange current density (i.e., j_0), which represents the ORR kinetics at the interface, was deduced from both the polarization curve and impedance spectra. The value is typically determined from the relationship between the polarization loss and current density, i.e., the Tafel equation. The activation loss at the electrode, which is mostly a cathodic contribution, is calculated from the polarization curve by eliminating the measured voltage and ohmic loss from the theoretical OCV as follows:

$$\eta_{act} = \mathrm{OCV} - V_{meas} - j \cdot ASR_e \quad [1]$$

Here, η_{act} is the activation loss, V_{meas} is the measured voltage during the experiment, and $j \cdot ASR_e$ is the ohmic loss. In addition, when the current density (j) is greater than j_0, the activation loss can be expressed as follows:

$$\eta_{act} = -\frac{RT}{\alpha n F}\ln j_0 + \frac{RT}{\alpha n F}\ln j \quad [2]$$

Here, R is the ideal gas constant, T is the absolute temperature, α is the coefficient of charge transfer, n is the number of electrons participating in the electrochemical reaction, and F is the Faraday constant. Figure 6 suggests the cathode surface kinetics with a relationship between the activation loss and current density by calculating j_0 from the y-axis intercept of the linear interpolation. The calculated values of j_0 for each fuel cell are 9.873, 8.525, and 2.858 mA/cm^2 for the 15 nm thick GDC capping layer, 50 cm thick GDC capping layer, and pure Pt cathodes, respectively. This tendency of the calculated exchange current density shows that the enhanced performance in terms of peak power density for fuel cells with a GDC capped cathode is a result of the increased cathode surface kinetics, represented by the ORR kinetics.

To highlight the electrochemical and thermo-stability of the fabricated fuel cell samples, we measured the voltage-output current density at 450°C for more than 25 hours. The voltage condition in the experiment was maintained at 0.5 V and the drained current densities are plotted in Figure 7. The fuel cell with the pure Pt cathode shows a dramatic drop of the current density within 10 hours

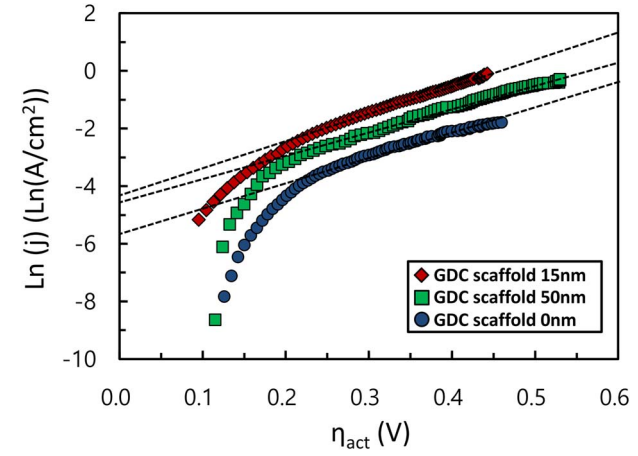

Figure 6. Tafel plots for the GDC oxide-capping layer and control fuel cells.

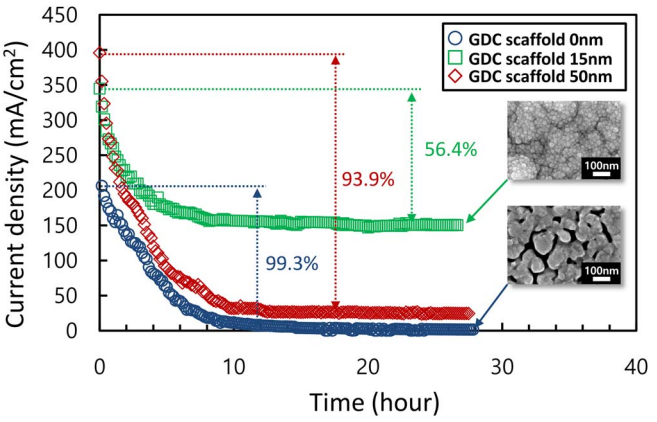

Figure 7. Stability test results of the GDC oxide-capped and pristine fuel cells over 25 hours at 450°C.

maintaining only 0.7% of its initial performance (i.e., 99.3% degradation), demonstrating the harsh degradation of the cathode by coarsening its morphological structure. However, the fuel cells coated with a GDC oxide-capping layer appeared to improve the durability compared to the pristine Pt cathode fuel cell. In particular, an outstanding improvement of stability was obtained in the case of the fuel cell with the 50 nm thick GDC capping layer. The fuel cell with the 15 nm capped GDC barely maintained its performance with a 93.9% degraded current density due to the insufficient capping as depicted in the SEM image in the inset of Figure 7. We also confirmed this in the SEM and TEM images shown in Figures 1 and 3. In the case of the 50 nm thick GDC capped fuel cell, it only showed 56.4% degradation in terms of power density, which demonstrates that the nano-porous Pt cathode maintained the structure and secured the TPB sites. It is thus believed that the degraded performance of the 50 nm thick GDC capping layer resulted in an un-penetrated part of nano grains for the Pt cathode, causing effective coarsening of its structure. Despite the remaining issues, the enhanced thermo-electrochemical stability obtained by applying a GDC capping layer supports application of this method beyond improvement of the metal cathode.

Conclusions

Despite using a PVD technique, it was shown that the GDC oxide-capping layers successfully function as a thermal barrier layer in this study. The GDC capping layers fabricated by sputtering enable the production of passive layers for the top morphology of the Pt cathode enhancing the ORR kinetics and thermo-stable behavior as well. The resulting GDC-capped fuel cell had a peak power density of 258 mW/cm^2 and significantly improved thermal stability during 25 hours of operation at 450°C. The results in this study are applicable to further studies of thermal barrier coatings and energy conversion devices, suggesting a novel method of blocking the coarsening metal electrode.

Acknowledgments

Y.B.K. gratefully acknowledges financial support from Hanyang Industrial Park at Hanyang University (contract#: 201300000001479).

References

1. B. Steele, *J. Power Sources*, **49**(1), 1 (1994).
2. B. Steele and A. Heinzel, *Nature*, **414**(6861), 345 (2001).
3. J. H. Shim, C.-C. Chao, H. Huang, and F. B. Prinz, *Chem. Mater.*, **19**(15), 3850 (2007).
4. P.-C. Su, C.-C. Chao, J. H. Shim, R. Fasching, and F. B. Prinz, *Nano Lett.*, **8**(8), 2289 (2008).
5. C.-C. Chao, Y. B. Kim, and F. B. Prinz, *Nano Lett.*, **9**(10), 3626 (2009).
6. J. Bae, S. Hong, B. Koo, J. An, F. B. Prinz, and Y.-B. Kim, *J. Eur. Ceram. Soc.*, **34**(15), 3763 (2014).
7. S. Hong, J. Bae, B. Koo, and Y.-B. Kim, *Electrochem. Commun.*, **47**, 1 (2014).
8. J. An, Y.-B. Kim, T. M. Guür, and F. B. Prinz, *ACS Appl. Mater. Interfaces*, **4**(12), 6790 (2012).
9. J. An, Y.-B. Kim, J. Park, T. M. Guür, and F. B. Prinz, *Nano Lett.*, **13**(9), 4551 (2013).
10. S. Hong, D. Lee, Y. Lim, J. Bae, and Y.-B. Kim, *Ceram. Int.*, **42**(15), 16703 (2016).
11. E. O. Oh, C. M. Whang, Y. R. Lee, S. Y. Park, D. H. Prasad, K. J. Yoon, J. W. Son, J. H. Lee, and H. W. Lee, *Adv. Mater.*, **24**(25), 3373 (2012).
12. H.-S. Noh, J.-W. Son, H. Lee, H.-S. Song, H.-W. Lee, and J.-H. Lee, *J. Electrochem. Soc.*, **156**(12), B1484 (2009).
13. Z.-P. Li, M. Toshiyuki, G. J. Auchterlonie, J. Zou, and D. John, *ACS Appl. Mater. Interfaces*, **3**(7), 2772 (2011).
14. Y. Chen, Y. Zhang, J. Baker, P. Majumdar, Z. Yang, M. Han, and F. Chen, *ACS Appl. Mater. Interfaces*, **6**(7), 5130 (2014).
15. W. Yang, T. Hong, S. Li, Z. Ma, C. Sun, C. Xia, and L. Chen, *ACS Appl. Mater. Interfaces*, **5**(3), 1143 (2013).
16. D. Rembelski, J.-P. Viricelle, L. Combemale, and M. Rieu, *Fuel Cells*, **12**(2), 256 (2012).
17. M. Balaguer, V. Vert, L. Navarrete, and J. Serra, *J. Power Sources*, **223**, 214 (2013).
18. H. Huang, M. Nakamura, P. Su, R. Fasching, Y. Saito, and F. B. Prinz, *J. Electrochem. Soc.*, **154**(1), B20 (2007).
19. Y. B. Kim, T. P. Holme, T. M. Gür, and F. B. Prinz, *Adv. Funct. Mater.*, **21**(24), 4684 (2011).
20. Y. B. Kim, J. H. Shim, T. M. Gür, and F. B. Prinz, *J. Electrochem. Soc.*, **158**(11), B1453 (2011).
21. G. Y. Cho, Y. H. Lee, S. W. Hong, J. Bae, J. An, Y. B. Kim, and S. W. Cha, *Int. J. Hydrogen Energy*, **40**(45), 15704 (2015).
22. A. Evans, A. Bieberle-Hütter, H. Galinski, J. L. Rupp, T. Ryll, B. Scherrer, R. Tölke, and L. J. Gauckler, *Monatsh. Chem.*, **140**(9), 975 (2009).
23. H. Galinski, T. Ryll, P. Elser, J. Rupp, A. Bieberle-Hütter, and L. Gauckler, *Phys. Rev. B*, **82**(23), 235415 (2010).
24. G. Y. Cho, Y. H. Lee, and S. W. Cha, *Renewable Energy*, **65**, 130 (2014).
25. X. Wang, H. Huang, T. Holme, X. Tian, and F. B. Prinz, *J. Power Sources*, **175**(1), 75 (2008).
26. K. Kerman, B.-K. Lai, and S. Ramanathan, *J. Power Sources*, **196**(5), 2608 (2011).
27. W. Jung, J. J. Kim, and H. L. Tuller, *J. Power Sources*, **275**, 860 (2015).
28. T. M. Onn, S. Zhang, L. Arroyo-Ramirez, Y.-C. Chung, G. W. Graham, X. Pan, and R. J. Gorte, *ACS Catal.*, **5**(10), 5696 (2015).
29. Y. K. Li, H. J. Choi, H. K. Kim, N. K. Chean, M. Kim, J. Koo, H. J. Jeong, D. Y. Jang, and J. H. Shim, *J. Power Sources*, **295**, 175 (2015).
30. K.-Y. Liu, L. Fan, C.-C. Yu, and P.-C. Su, *Electrochem. Commun.*, **56**, 65 (2015).
31. K. C. Neoh, G. D. Han, M. Kim, J. W. Kim, H. J. Choi, S. W. Park, and J. H. Shim, *Nanotechnology*, **27**(18), 185403 (2016).
32. I. Chang, S. Ji, J. Park, M. H. Lee, and S. W. Cha, *Adv. Energy Mater.*, **5**(10), 1402251 (2015).
33. J. A. Thornton and D. Hoffman, *Thin Solid Films*, **171**(1), 5 (1989).
34. P. Briois, F. Lapostolle, V. Demange, E. Djurado, and A. Billard, *Surf. Coat. Technol.*, **201**(12), 6012 (2007).
35. Y. H. Lee, G. Y. Cho, I. Chang, S. Ji, Y. B. Kim, and S. W. Cha, *J. Power Sources*, **307**, 289 (2016).
36. H. J. Choi, M. Kim, K. C. Neoh, D. Y. Jang, H. J. Kim, J. M. Shin, G.-T. Kim, and J. H. Shim, *Adv. Energy. Mater.*, **7**(4), 1601956 (2016).
37. C.-C. Yu, S. Kim, J. D. Baek, Y. Li, P.-C. Su, and T.-S. Kim, *ACS Appl. Mater. Interfaces*, **7**(11), 6036 (2015).